ACS APPLIED MATERIALS & INTERFACES

Research Article

www.acsami.org

Nitrogen-Doped Graphene Aerogels as Efficient Supercapacitor Electrodes and Gas Adsorbents

Zhu-Yin Sui, Yue-Na Meng, Pei-Wen Xiao, Zhi-Qiang Zhao, Zhi-Xiang Wei,* and Bao-Hang Han*

National Center for Nanoscience and Technology, Beijing 100190, China

Supporting Information

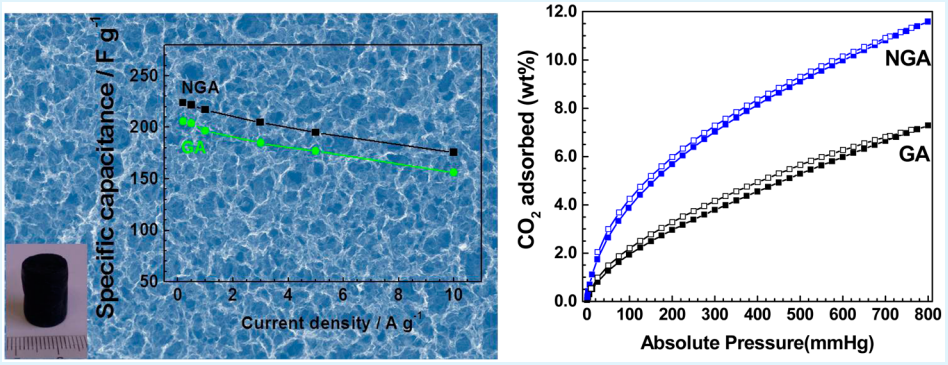

ABSTRACT: Nitrogen-doped graphene has been demonstrated to be an excellent multifunctional material due to its intriguing features such as outstanding electrocatalytic activity, high electrical conductivity, and good chemical stability as well as wettability. However, synthesizing the nitrogen-doped graphene with a high nitrogen content and large specific surface area is still a challenge. In this study, we prepared a nitrogen-doped graphene aerogel (NGA) with high porosity by means of a simple hydrothermal reaction, in which graphene oxide and ammonia are adopted as carbon and nitrogen source, respectively. The microstructure, morphology, porous properties, and chemical composition of NGA were well-disclosed by a variety of characterization methods, such as scanning electron microscopy, nitrogen adsorption−desorption measurements, X-ray photoelectron spectroscopy, and Raman spectroscopy. The as-made NGA displays a large Brunauer−Emmett−Teller specific surface area (830 $m^2 g^{-1}$), high nitrogen content (8.4 atom %), and excellent electrical conductivity and wettability. On the basis of these features, the as-made NGA shows superior capacitive behavior (223 F g^{-1} at 0.2 A g^{-1}) and long-term cycling performance in 1.0 mol L^{-1} H_2SO_4 electrolyte. Furthermore, the NGA also possesses a high carbon dioxide uptake capacity at 1.0 bar and 273 K (11.3 wt %).

KEYWORDS: *graphene, supercapacitor, porous material, aerogel, adsorbent*

INTRODUCTION

Aerogels, usually obtained from the supercritical carbon dioxide drying or freeze-drying of the wet gels to replace the solvents with air, are three-dimensional (3D) porous solid materials and present many intriguing physical properties, including high porosity, excellent mass-transfer capability, and low bulk density and dielectric permittivity.[1,2] Since Kistler et al. reported the preparation of silica aerogels in 1931,[3] aerogels with porosity have been obtained from many starting materials, such as metal oxides and metal chalcogenides.[4−6] Carbonaceous aerogels assembled of carbon nanostructures have shown potential in many fields, such as sorption, catalysis, and electrode materials.[7−10] This is because carbon materials are lightweight and possess an extraordinary mechanical, thermal, and chemical stability as well as tunable electrical properties.[11]

Graphene, a two-dimensional carbon nanomaterial, possesses many outstanding properties, such as large specific surface area, excellent chemical stability, and superior optical and electrical properties.[12] Recently, graphene-based porous materials have been extensively explored and held promise in the fields of catalysis,[13−15] energy storage,[16,17] and gas adsorption.[18−20] Various methods have been applied to prepare graphene-based porous materials, such as covalent or noncovalent cross-linking,[21,22] chemical or physical activation,[23−25] in situ reduction,[26,27] and template-directing methods.[28,29] Graphene-based aerogels, one of graphene-based porous materials, can not only inherit graphene's outstanding intrinsic properties but also possess large specific surface area and pore volume. Graphene-based aerogels with high porosity and an interconnected network have been developed to improve material performance.[30] For example, a mechanically strong and electrically conductive graphene aerogel reported by Zhang et al. was prepared by supercritical drying of hydrogel precursor synthesized from reduction of aqueous graphene oxide (GO)

Received: June 28, 2014
Accepted: December 29, 2014
Published: December 29, 2014

DOI: 10.1021/am5042065
ACS Appl. Mater. Interfaces 2015, 7, 1431−1438

dispersion with L-ascorbic acid.[26] The as-prepared graphene aerogel displayed a specific capacitance of 128 F g^{-1} at a current density of 50 mA g^{-1}. Cong et al. reported a facile method of the fabrication of a multifunctional graphene-based aerogel with interconnected porous networks using ferrous ions as a reducing agent.[31] The as-prepared graphene-based aerogel exhibited an excellent adsorption performance for the removal of heavy ions and oils. In our previous report, we also prepared a similar material via the interaction between GO sheets and polyethylenimine.[32] The obtained porous materials displayed an extremely high adsorption capacity for the removal of dyes and the adsorption of carbon dioxide.

Nitrogen-doped graphene (NG) has been widely investigated owing to its high electrical conductivity, large specific surface area, and good chemical stability.[24,33−35] For example, Sheng et al. prepared an NG through a thermal annealing approach of GO using melamine as the nitrogen source, which showed improved conductivity and excellent electrocatalytic activity.[36] Zhao et al. reported an ultralight NG framework, which displayed a greatly high capacitance of 484 F g^{-1} and can be used as a metal-free catalyst for oxygen reduction.[37] However, relatively low specific surface area, poor yield, or complex processes largely limited their practical use. Research on nitrogen-doped graphene-based aerogel is ongoing. It is expected that the introduction of nitrogen species into graphene aerogel can largely adjust the chemical attribute and electrical property, thus improving the material's performance. For example, Yin et al. demonstrated that a nitrogen-doped graphene-based hybrid aerogel prepared through a facile hydrothermal method showed excellent catalytic activity in oxygen reduction.[38] Zhang et al. reported nitrogen-doped activated graphene aerogel/gold nanoparticles, which showed excellent electrochemical response to hydroquinone and *o*-dihydroxybenzene.[39] Nevertheless, the work on nitrogen-doped graphene aerogels as supercapacitor electrode materials and gas adsorbents has never been reported to date.

In this work, we present a facile method to the preparation of nitrogen-doped graphene aerogel (NGA), in which GO and ammonia are adopted as carbon and nitrogen sources, respectively. The NGA with excellent electrical conductivity and high nitrogen level (8.4 atom %) displays a porous network structure with high porosity. On the basis of the dual advantages of aerogels and nitrogen-doped graphene, the NGA material exhibits high specific capacitance (223 F g^{-1} at 0.2 A g^{-1}), good rate performance, and long-term cycling stability. Furthermore, the NGA also possesses a high carbon dioxide uptake capacity at 1.0 bar and 273 K (11.3 wt %). To the best of our knowledge, this is the first report to use nitrogen-containing graphene aerogels as gas adsorbents. The excellent performance can be attributed to the porous properties of aerogels and the introduction of nitrogen species.

EXPERIMENTAL SECTION

Preparation of Nitrogen-Doped Graphene Aerogel. In a typical experiment, graphite oxide was obtained from the natural flake graphite (99 wt % purity, average particle diameter of 20 μm, Yingshida graphite Co. Ltd., Qingdao, China) through a modified Hummers' method.[40,41] The as-prepared graphite oxide was fully washed using plenty of ultrapure water, followed by sonicating it in water for 60 min to obtain aqueous GO dispersion. Aqueous GO dispersion (18 mL, 5 mg mL^{-1}) and 4 mL of ammonia solution (28 wt %, Beijing Chemical Reagents Company) were sealed in a Teflon-lined stainless-steel autoclave, subsequently heating the mixture at 180 °C for 12 h, thus forming a hydrogel. After the as-prepared hydrogel was dialyzed with ultrapure water for 3 d followed by freeze-drying, the NGA was obtained. For comparison, graphene aerogel (GA) was prepared in a similar method without the addition of ammonia.

Instrumental Characterization. The adsorption isotherms of all gases (nitrogen, carbon dioxide, and methane) were performed with a TriStar II 3020 surface area and porosity analyzer (Micromeritics Instrument Corporation, U.S.A.). The as-prepared porous materials were degassed at 120 °C for 24 h prior to measurements. Nitrogen adsorption−desorption measurements were carried out at 77 K to give the pore parameters. The carbon dioxide and methane adsorption isotherms were conducted at 273 K. Scanning electron microscopy (SEM) images were obtained from a Hitachi S-4800 field emission scanning electron microscope (Hitachi Ltd., Japan), whereas transmission electron microscopy (TEM) images were taken with a Tecnai G^2 20 S-TWIN microscope (FEI, U.S.A.) operating at 200 kV. The samples were dispersed in ethanol, followed by sonicating the mixture for 60 min. Then the resultant dispersions were dropped on a copper grid and dried overnight at room temperature. Thermal gravimetric analysis (TGA) was carried out on a Pyris Diamond thermogravimetric/differential thermal analyzer at a heating rate of 10 °C min^{-1} in nitrogen atmosphere. Raman spectra were measured on a Renishaw inVia Raman spectrometer (Renishaw plc, U.K.) with a laser of a wavelength of 514 nm at room temperature. X-ray diffraction (XRD) patterns were measured by a Philips X'Pert PRO X-ray diffraction instrument using Cu Kα radiation. X-ray photoelectron spectroscopy (XPS) was conducted on an ESCALab220i-XL electron spectrometer (VG Scientific Ltd., U.K.) using Al Kα radiation at 300 W. Infrared spectrum was conducted on PerkinElmer Fourier transform infrared (FTIR) spectroscopy instruments (U.S.A.). The electrical conductivity (two-probe method) was measured on a Keithley 4200 Semiconductor Characterization System, and silver paste was applied to make a good contact between the probe and sample.

Electrodes were fabricated by mixing 85 wt % active material, 5 wt % polytetrafluoroethylene (PTFE 60 wt % dispersion in water, Sigma-Aldrich), and 10 wt % conducting carbon black. All electrochemical experiments were performed in two-electrode sandwich type-cells using a gold grid as the current collector. Electrochemical supercapacitor was assembled using two working electrodes, electrically isolated by a glassy fibrous separator. Aqueous H_2SO_4 solution (1.0 mol L^{-1}) was used as electrolyte. The electrochemical performances of the as-made electrodes were analyzed by cyclic voltammetry (CV) tests, galvanostatic charge−discharge cycling, as well as electrochemical impedance spectroscopy. CV and galvanostatic charge−discharge cycling were performed in the 0−1 V potential range. All the electrochemical experimental experiments mentioned above were carried out using a computer-controlled EG&G Princeton Applied Research VMP3 workstation.

RESULTS AND DISCUSSION

In a typical preparation process, the mixture of aqueous GO dispersion (18 mL, 5 mg mL^{-1}) and ammonia (4 mL) were added into a sealed Teflon-lined stainless-steel autoclave and transferred into an oven. The above mixture can form a black hydrogel with a cylinder shape (Figure S1, Supporting Information) after the hydrothermal treatment at 180 °C for 12 h. The as-prepared hydrogel contained approximately 2.9 wt % of nitrogen-doped graphene and 97.1 wt % of water. The NGA was prepared through freeze-drying of the as-made hydrogel for 24 h under vacuum condition to obtain a highly porous material.[27,42] After freeze-drying, the NGA showed a low density (~80 mg cm^{-3}) calculated by the mass of the NGA divided by its volume. The morphology and structure of the as-prepared NGA were studied by means of SEM, TEM, XRD, and Raman spectroscopy. The SEM images as shown in Figure 1a,b clearly show that the NGA exhibits a hierarchical and interconnected porous network composed of randomly oriented graphene sheets, similar to those of previous graphene

DOI: 10.1021/am5042065
ACS Appl. Mater. Interfaces 2015, 7, 1431−1438

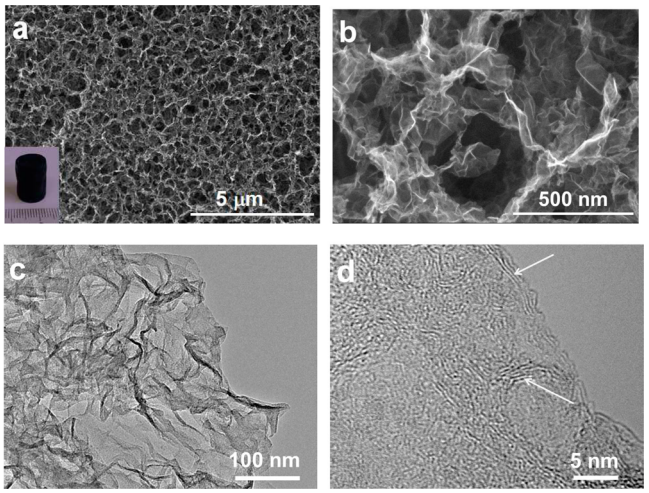

Figure 1. (a, b) SEM images of nitrogen-doped graphene aerogel at different magnifications, (c, d) TEM images of NGA at different magnifications. Inset: a digital photo of the NGA.

aerogels.[26,30] It can be clearly observed that the pore size varies from tens of nanometers to several hundred nanometers. The unique 3D porous structure can largely prevent the aggregation of graphene sheets caused by $\pi-\pi$ interaction and van der Waals force, which may be beneficial to the rapid transport of electrolyte.[42] The TEM image (Figure 1c) also reveals that the NGA has a unique interconnected porous nanostructure, and curved sheets can also be clearly seen. Figure 1d shows that the NGA mainly exhibits an amorphous structure, and some locally ordered structure pointed out by the white arrow can be observed. The above-mentioned analyses confirm that we prepared a material with porous microstructure.

The wide-angle powder XRD patterns of the as-prepared porous materials are displayed in Figure S2 (Supporting Information). GO has a large interlayer distance (0.78 nm, 2θ = 11.6°) according to the (002) diffraction peak. The expanded interlayer spacing in comparison with that of graphite (0.34 nm) confirms the presence of oxygenated functional groups on GO sheets.[41] After the hydrothermal reduction, the peak at 2θ = 11.6° completely disappears, while a weak and broad peak centered at ~24° corresponding to the interlayer distance of ca. 0.37 nm emerges in the GA and NGA, indicating the partial reduction of GO.[26] Compared with GO, the reduced interlayer spacing in NGA indicates that most oxygen-containing functional groups introduced into the interlayer spacing of graphite can be removed during the hydrothermal process. To study the structure of these graphene-based carbon materials further, the as-made porous materials were analyzed by Raman spectra (Figure S3, Supporting Information). The characteristic D-band (1350 cm^{-1}) and G-band (1590 cm^{-1}) can be observed for the NGA, GA, and GO.[19] The increased defects and the reduced size of sp^2 domain can be confirmed by the increasing values of D-band/G-band intensity ratios in the GA (0.98) and NGA (0.97) compared with that of GO (0.80), which is in accordance with the previous results.[43]

The types and content of nitrogen species can be characterized by XPS. As shown in Figure 2a, all of these samples show C 1s and O 1s. However, the NGA shows an additional N 1s, indicating the successful introduction of nitrogen. The nitrogen content is 8.4 atom %. The N 1s spectrum (Figure 2b) can be deconvolved into three types, namely, 398.7, 399.9, and 401.8 eV, corresponding to the pyridinic, pyrrolic, and quaternary nitrogen, respectively.[44] Figure 2c displays the high-resolution XPS C 1s spectra of these samples, which contain graphitic carbon at 284.8 eV, C−O (epoxyl and hydroxyl) at 286.8 eV, carbonyl at 287.9 eV, and

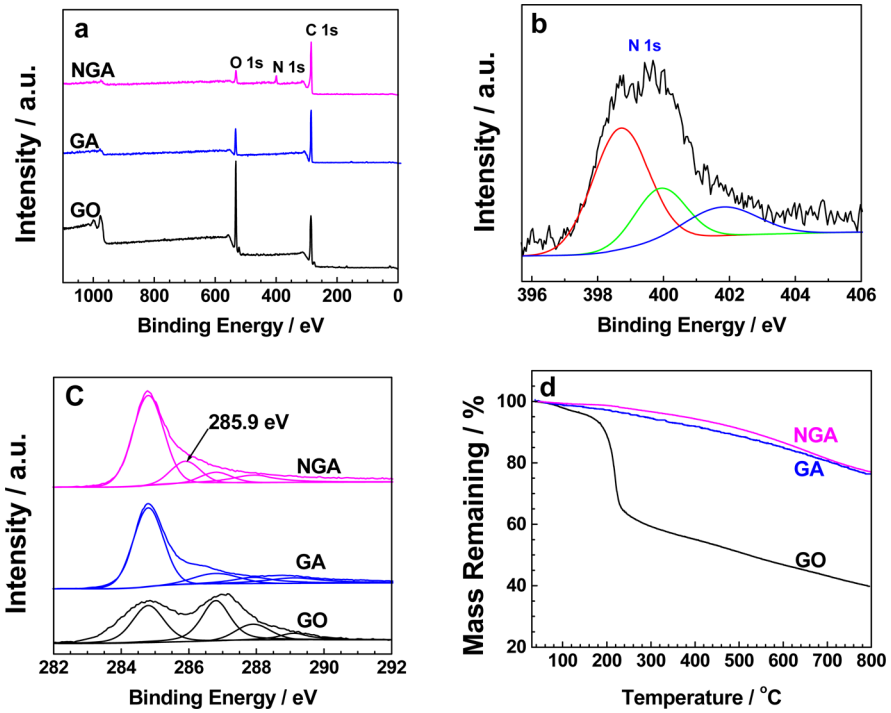

Figure 2. (a) XPS spectra of graphene oxide (GO), graphene aerogel (GA), and nitrogen-doped graphene aerogel (NGA), (b) N 1s spectra of the NGA, (c) C 1s spectra, and (d) thermal gravimetric analysis curves of GO, GA, and NGA.

DOI: 10.1021/am5042065
ACS Appl. Mater. Interfaces 2015, 7, 1431−1438

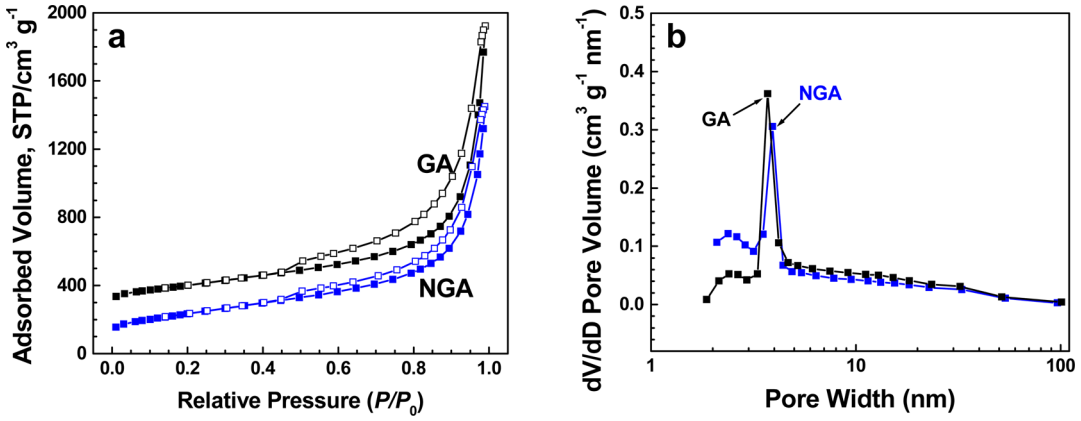

Figure 3. (a) Typical nitrogen adsorption−desorption isotherms and (b) Barret−Joyner−Halenda desorption pore size distribution profiles of nitrogen-doped graphene aerogel (NGA) and graphene aerogel (GA). The isotherm of GA was offset by 200 units to make curves clear. (■ for adsorption and □ for desorption in the nitrogen sorption isotherms.).

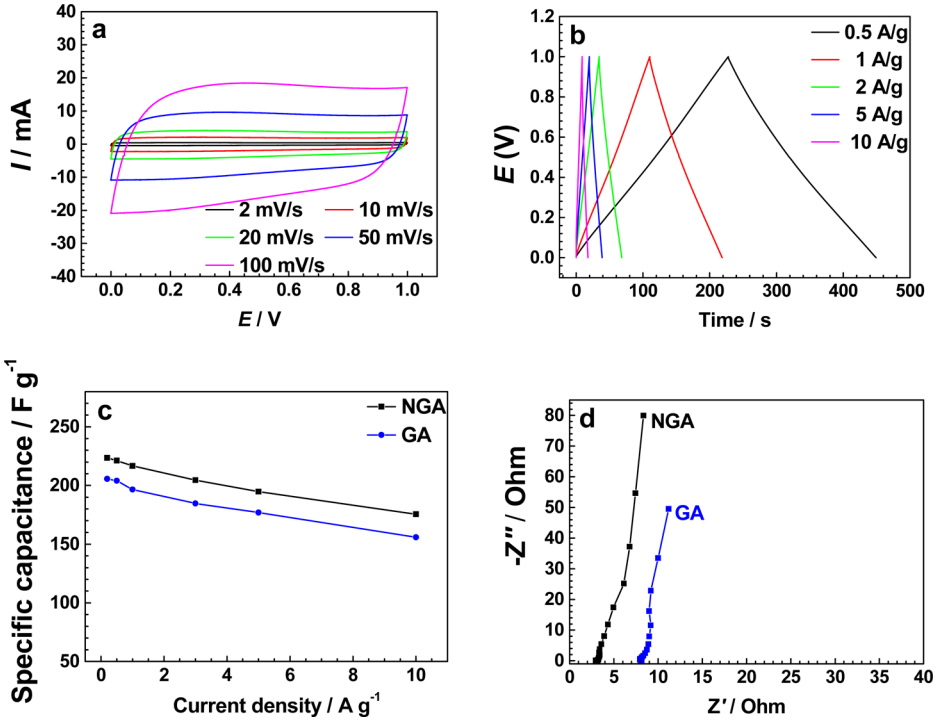

Figure 4. (a) Cyclic voltammetry curves of nitrogen-doped graphene aerogel (NGA) in 1.0 mol L^{-1} H_2SO_4 electrolyte at different scan rates, (b) galvanostatic charge−discharge curves of NGA at different current densities, (c) specific capacitances of NGA and GA as a function of discharge current density, and (d) Nyquist plots of NGA and GA.

carboxyl at 289.1 eV.[26] There is an obvious decrease in the amount of oxygen-containing functional groups during the hydrothermal reduction of GO, which is in accordance with the XRD results. The peak of NGA located at 285.9 eV can be attributed to C−N bonds.[45] Seen from Table S2 (Supporting Information), the oxygen content decreases from 33.1 atom % for GO to 15.1 atom % for GA to 9.2 atom % for NGA, indicating that the addition of ammonia can enhance the reduction of GO. The reduction of GO was also detected by the FTIR spectra (Figure S4, Supporting Information). For GO, there is an absorption band at 1720 cm^{-1}, which is ascribed to C═O stretching vibrations in carboxyl and carbonyl. For NGA and GA, the intensity of C═O peak decreases obviously after hydrothermal treatment, further indicating the successful reduction of GO. In addition, the thermal decomposition of GO, GA, and NGA was characterized by thermal gravimetric analysis. Seen from Figure 2d, there is a significant increase in the thermal stability for NGA and GA samples owing to the decrease in the amount of oxygenated functional groups.

The porous characteristics of the NGA were characterized by nitrogen adsorption−desorption experiments. The nitrogen adsorption−desorption isotherms and pore size distributions of NGA and GA are shown in Figure 3. Both GA and NGA possess type IV isotherms with type H3 hysteresis at 0.45−1.0 relative pressure range, indicating the presence of mesoporosity and slit-shaped pores.[26] The NGA exhibits a Brunauer−Emmett−Teller (BET) specific surface area of 830 m^2 g^{-1}, which is superior to those of most graphene-based porous materials, for example, 3D nitrogen-doped graphene (280 m^2

DOI: 10.1021/am5042065
ACS Appl. Mater. Interfaces 2015, 7, 1431−1438

g^{-1})[37] and graphene aerogel (510 m^2 g^{-1}).[26] However, the specific surface area of the NGA is still less than the theoretical value (2600 m^2 g^{-1}) for graphene sheets, indicating the stacking of graphene sheets within the as-prepared porous material, which matches well with the result of XRD. Figure 3b depicts the pore size distributions of NGA and GA according to the Barret–Joyner–Halenda (BJH) method, which displays that most pore volume of NGA lies in the 2–30 nm region and that the main peak centers at ~3.9 nm. Table S1 (Supporting Information) gives the textural parameters of the as-made porous materials, including specific surface area, pore volume, and pore diameter.

Electrical conductivity of NGA and GA was measured by a two-probe method. It was found that NGA (0.8 S m^{-1}) has higher conductivity than GA (0.5 S m^{-1}). The improved electrical conductivity can be explained by the lower oxygen content in NGA compared with GA, implying the addition of ammonia during hydrothermal treatment leads to the enhancement of GO reduction degree. In addition, the wettability of the as-made porous materials was also studied. All these wettability experiments were conducted at room temperature. Before test, NGA or GA was pressed into a round cake at a pressure of 25 MPa. Water (5 μL) was dropped onto the surface of samples. It was found that NGA sample (~2 min) needed shorter time to be fully infiltrated by the water droplet compared with GA sample (~8 min), which suggests that NGA possesses better wettability than GA. It can be seen from Table S2 (Supporting Information) that NGA (17.6 atom %) displays a higher content of nitrogen and oxygen than GA (15.1 atom %). The increased wettability of NGA can be ascribed to the high relative content of nitrogen and oxygen, which can facilitate hydrogen bonding between nitrogen or oxygen atom and the water molecules.[46]

To explore the NGA as supercapacitor electrode, the capacitive performance of the NGA was measured by using a two-electrode system in 1.0 mol L^{-1} H_2SO_4 electrolyte. Figure 4a and Figure S5a (Supporting Information) exhibit the cyclic voltammetry (CV) curves of NGA and GA at different scan rates. It can be evidently found that all of the CV curves show a quasi-rectangular shape and no significant change with the increase in scan rates, suggesting the excellent rate capacity of NGA. Even when the scan rate increases to 100 mV s^{-1}, the CV curves of the NGA and GA still remain a quasi-rectangular shape with a slight deviation at lower potential, indicating a quick charge propagation capacity. The rate performances of the NGA and GA were evaluated by galvanostatic charge–discharge under different current densities. Seen from Figure 4b and Figure S5b (Supporting Information), the voltage–time curves of the NGA and GA show an ideal linear shape, suggesting their excellent electrical performances. On the basis of the slope of the discharge curve, the specific capacitance of the NGA electrode reaches ~223 F g^{-1} at a current density of 0.2 A g^{-1}, which is superior to those of some other porous materials at the same current density.[26,47] Furthermore, the superior capacitance of the NGA is preserved at higher current density as shown in Figure 4c. Even when the current density increases to 10 A g^{-1}, the specific capacitance of NGA electrode still reaches 176 F g^{-1}, corresponding to 78% capacitance retention compared with the capacitance at 0.2 A g^{-1}. The GA electrode exhibits ~75% capacitance retention with the same increase in the current density, indicating that the well-defined porous structure of the as-prepared aerogels (NGA and GA) is an important factor for efficient ion diffusion, especially at the large current density. Compared with GA electrode, the enhanced specific capacitance for the NGA could be ascribed to the good wettability and electrical conductivity, which can facilitate the electrolyte permeation and electron transport.[33,47] In addition, the Nyquist plots of NGA and GA are given in Figure 4d. The plots of NGA and GA electrodes feature a vertical line in a low-frequency region, indicating a nearly ideal capacitive behavior. The real-axis intercept is considered to be the equivalent series resistance (ESR) in a high-frequency region. Figure 4d indicates that the NGA has lower ESR than that of GA, suggesting that the NGA with excellent electrical conductivity can reduce the charge-transfer resistance, which is beneficial to the electrochemical performance.

The cycling stability is an important indicator in the practical application of electrode materials, so we further studied the cycling performance of the NGA.[48] Figure 5 shows cycling stability of the NGA, which was investigated at a charge–discharge current density of 1.0 A g^{-1}. It can be seen that the NGA shows an outstanding cycling stability and exhibits a slight decrease (8%) in the specific capacitance after 2000 cycles. Compared with the electrochemical properties of other pseudocapacitive materials, such as manganese dioxide-based carbonaceous electrodes[49,50] and conductive polymers,[51] the excellent capacitive behaviors indicate that these functional groups of NGA are greatly stable and considerably reversible during the charge–discharge cycling process. The above-mentioned results indicate that the as-made NGA is a promising electrode material as supercapacitor. The outstanding electrochemical performance can be ascribed to the well-developed hierarchical porous structure, excellent electrical conductivity, the uniformly dispersed functional groups covalently bonded on the graphene sheets, and high nitrogen content.

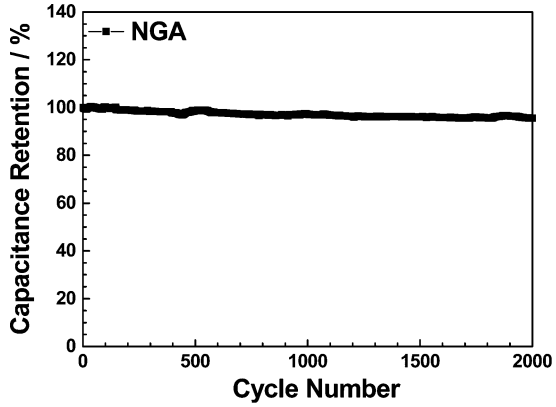

Figure 5. Cycling stability of nitrogen-doped graphene aerogel at a charge–discharge current density of 1.0 A g^{-1} for 2000 cycles.

The porous NGA with the high nitrogen content will probably interact attractively with some gas molecules through the enhanced molecular interaction.[52] Therefore, we investigated the gas (carbon dioxide and methane) adsorption performance of NGA. Figure 6a shows the carbon dioxide adsorption–desorption isotherms of both NGA and GA at 273 K. The GA displays moderate adsorption capacity for carbon dioxide (7.1 wt % at 1.0 bar and 273 K). We can see that there is a large enhancement in carbon dioxide adsorption capacity for NGA (11.3 wt %), which is superior to other porous materials at the same condition.[32,53,54]

DOI: 10.1021/am5042065
ACS Appl. Mater. Interfaces 2015, 7, 1431–1438

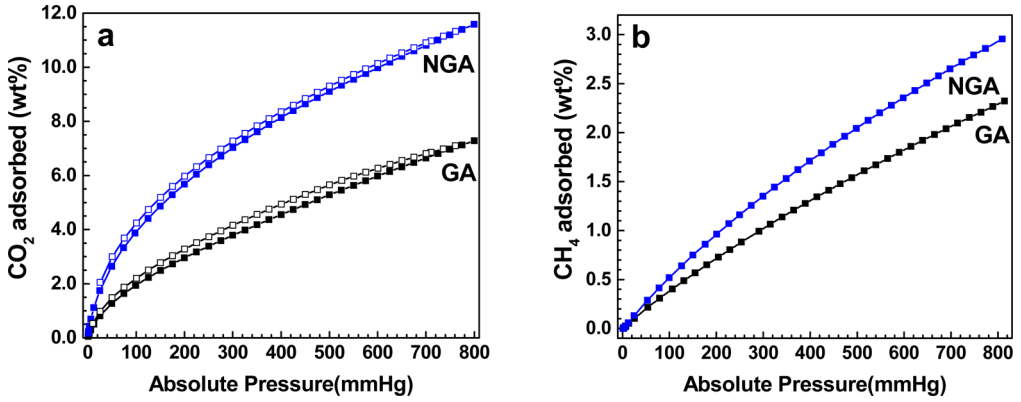

Figure 6. (a) Carbon dioxide sorption isotherms at 273 K of graphene aerogel (GA) and nitrogen-doped graphene aerogel (NGA); ■ for adsorption and □ for desorption. (b) Methane adsorption isotherms at 273 K of GA and NGA.

In addition, the carbon dioxide adsorption−desorption isotherm of the NGA is nearly reversible, suggesting that the carbon dioxide uptake is basically through physisorption or weak interaction. The methane uptake of the NGA was also studied as seen from Figure 6b. At 1.0 bar and 273 K, the NGA exhibits a higher uptake capacity (2.8 wt %) than that (2.2 wt %) of GA, which is comparable to some highly porous materials, such as fluorinated porous organic polymers,[55] adamantine-based porous polymer networks,[56] and microporous polycarbazole CPOP-1 under the same conditions.[52] In addition, the selectivity of NGA toward carbon dioxide over nitrogen was also investigated at 273 K as given in Figure S6 (Supporting Information). At 1.0 bar and 273 K, the carbon dioxide and nitrogen adsorption capacity of the NGA is 2.57 and 0.22 mmol g^{-1}, respectively. The estimated adsorption selectivity of carbon dioxide over nitrogen is 12. The excellent adsorption performance can be attributed to the high charge density at the nitrogen site of NGA, which might enhance the interaction with the polarizable carbon dioxide molecules via local dipole−quadrupole interaction.[52]

CONCLUSIONS

We have successfully prepared the NGA by means of a facile hydrothermal reaction, in which GO and ammonia are adopted as carbon and nitrogen source, respectively. The as-prepared NGA exhibits a 3D porous network structure with a large BET specific surface area (830 m^2 g^{-1}) and high nitrogen content (8.4 atom %). These features make the NGA material possess excellent electrochemical performance, including large specific capacitance (223 F g^{-1} at 0.2 A g^{-1}), outstanding capacity retention, and long-term cycling stability. The high performance of the NGA can be attributed to its unique structure. First, the hierarchical porous structure of the NGA with high porosity provides short ion transfer pathways during the process of charge−discharge. Second, the good electrical conductivity and wettability can facilitate the electron transport and electrolyte permeation, further improving its electrochemical performance. Furthermore, the NGA also possesses a high carbon dioxide adsorption capacity (11.3 wt % at 1.0 bar and 273 K) due to possessing large specific surface area and high nitrogen content. Thus, the as-prepared NGA could hold promise in the fields of energy and environment.

ASSOCIATED CONTENT

Supporting Information

Digital photos of the as-prepared hydrogel; XRD patterns; Raman and FTIR spectra of GO, GA, and NGA; cyclic voltammetry curves of GA at different scan rates; galvanostatic charge−discharge curves of GA at various current densities. This material is available free of charge via the Internet at http://pubs.acs.org.

AUTHOR INFORMATION

Corresponding Authors

*E-mail: hanbh@nanoctr.cn. Phone: +86 10 8254 5576. (B.H.H.)

*E-mail: weizx@nanoctr.cn. Phone: +86 10 8254 5565. (Z.X.W.)

Notes

The authors declare no competing financial interest.

ACKNOWLEDGMENTS

The financial support of the National Natural Science Foundation of China (Grant Nos. 21374024 and 61261130092), the Ministry of Science and Technology of China (Grant No. 2014CB932200), and the Chinese Academy of Sciences (Grant No. XXH12504-3-10) is acknowledged.

REFERENCES

(1) Pierre, A. C.; Pajonk, G. M. Chemistry of Aerogels and Their Applications. *Chem. Rev.* **2002**, *102*, 4243−4265.

(2) Hüsing, N.; Schubert, U. Aerogels—Airy Materials: Chemistry, Structure, and Properties. *Angew. Chem., Int. Ed.* **1998**, *37*, 22−45.

(3) Kistler, S. S. Coherent Expanded Aerogels and Jellies. *Nature* **1931**, *127*, 741−741.

(4) Signoretto, M.; Ghedini, E.; Menegazzo, F.; Cerrato, G.; Crocellà, V.; Bianchi, C. L. Aerogel and Xerogel WO_3/ZrO_2 Samples for Fine Chemicals Production. *Microporous Mesoporous Mater.* **2013**, *165*, 134−141.

(5) Zu, G. Q.; Shen, J.; Zou, L. P.; Wang, W. Q.; Lian, Y.; Zhang, Z. H.; Du, A. Nanoengineering Super Heat-Resistant, Strong Alumina Aerogels. *Chem. Mater.* **2013**, *25*, 4757−4764.

(6) Mohanan, J. L.; Arachchige, I. U.; Brock, S. L. Porous Semiconductor Chalcogenide Aerogels. *Science* **2005**, *307*, 397−400.

(7) Kabbour, H.; Baumann, T. F.; Satcher, J. H.; Saulnier, A.; Ahn, C. C. Toward New Candidates for Hydrogen Storage: High-Surface-Area Carbon Aerogels. *Chem. Mater.* **2006**, *18*, 6085−6087.

(8) Long, J. W.; Dunn, B.; Rolison, D. R.; White, H. S. Three-Dimensional Battery Architectures. *Chem. Rev.* **2004**, *104*, 4463−4492.

DOI: 10.1021/am5042065
ACS Appl. Mater. Interfaces 2015, 7, 1431−1438

(9) Rolison, D. R.; Dunn, B. Electrically Conductive Oxide Aerogels: New Materials in Electrochemistry. *J. Mater. Chem.* **2001**, *11*, 963−980.
(10) Moreno-Castilla, C.; Maldonado-Hódar, F. J. Carbon Aerogels for Catalysis Applications: an Overview. *Carbon* **2005**, *43*, 455−465.
(11) Titirici, M.-M.; Antonietti, M. Chemistry and Materials Options of Sustainable Carbon Materials Made by Hydrothermal Carbonization. *Chem. Soc. Rev.* **2010**, *39*, 103−116.
(12) Dreyer, D. R.; Ruoff, R. S.; Bielawski, C. W. From Conception to Realization: An Historial Account of Graphene and Some Perspectives for Its Future. *Angew. Chem., Int. Ed.* **2010**, *49*, 9336−9344.
(13) Zhang, L.; Shao, J.; Zhang, W.; Zhang, C.; Zheng, X.; Du, H.; Yang, Q. Graphene-Based Porous Catalyst with High Stability and Activity for the Methanol Oxidation Reaction. *J. Phys. Chem. C* **2014**, *118*, 25918−25923.
(14) Liu, X.; Antonietti, M. Moderating Black Powder Chemistry for the Synthesis of Doped and Highly Porous Graphene Nanoplatelets and Their Use in Electrocatalysis. *Adv. Mater.* **2013**, *25*, 6284−6290.
(15) Adhikari, B.; Biswas, A.; Banerjee, A. Graphene Oxide-Based Hydrogels to Make Metal Nanoparticle-Containing Reduced Graphene Oxide-Based Functional Hybrid Hydrogels. *ACS Appl. Mater. Interfaces* **2012**, *4*, 5472−5482.
(16) Gao, H.; Xiao, F.; Ching, C.; Duan, H. High-Performance Asymmetric Supercapacitor Based on Graphene Hydrogel and Nanostructured MnO_2. *ACS Appl. Mater. Interfaces* **2012**, *4*, 2801−2810.
(17) Sun, Y.; Wu, Q.; Shi, G. Graphene Based New Energy Materials. *Energy Environ. Sci.* **2011**, *4*, 1113−1132.
(18) Zhou, D.; Liu, Q.; Cheng, Q.-Y.; Zhao, Y.-C.; Cui, Y.; Wang, T.; Han, B.-H. Graphene-Manganese Oxide Hybrid Porous Material and its Application in Carbon Dioxide Adsorption. *Chin. Sci. Bull.* **2012**, *57*, 3059−3064.
(19) Zhou, D.; Han, B.-H. Graphene-Based Nanoporous Materials Assembled by Mediation of Polyoxometalate Nanoparticle. *Adv. Funct. Mater.* **2010**, *20*, 2717−2722.
(20) Chandra, V.; Yu, S. U.; Kim, S. H.; Yoon, Y. S.; Kim, D. Y.; Kwon, A. H.; Meyyappan, M.; Kim, K. S. Highly Selective CO_2 Capture on N-doped Carbon Produced by Chemical Activation of Polypyrrole Functionalized Graphene Sheets. *Chem. Commun.* **2012**, *48*, 735−737.
(21) Zhang, D.-D.; Zu, S.-Z.; Han, B.-H. Inorganic−Organic Hybrid Porous Materials Based on Graphite Oxide Sheets. *Carbon* **2009**, *47*, 2993−3000.
(22) Huang, H.; Lü, S. Y.; Zhang, X. T.; Shao, Z. Q. Glucono-δ-lactone Controlled Assembly of Graphene Oxide Hydrogels with Selectively Reversible Gel-Sol Transition. *Soft Matter* **2012**, *8*, 4609−4615.
(23) Zhu, Y.; Murali, S.; Stoller, M. D.; Ganesh, K. J.; Cai, W.; Ferreira, P. J.; Pirkle, A.; Wallace, R. M.; Cychosz, K. A.; Thommes, M.; Su, D.; Stach, E. A.; Ruoff, R. S. Carbon-Based Supercapacitors Produced by Activation of Graphene. *Science* **2011**, *332*, 1537−1541.
(24) Chandra, V.; Yu, S. U.; Kim, S. H.; Yoon, Y. S.; Kim, D. Y.; Kwon, A. H.; Meyyappan, M.; Kim, K. S. Highly Selective CO_2 Capture on N-doped Carbon Produced by Chemical Activation of Polypyrrole Functionalized Graphene Sheets. *Chem. Commun.* **2012**, *48*, 735−737.
(25) Sui, Z.-Y.; Meng, Q.-H.; Li, J.-T.; Zhu, J.-H; Cui, Y.; Han, B.-H. High Surface Area Porous Carbons Produced by Steam Activation of Graphene Aerogels. *J. Mater. Chem. A* **2014**, *2*, 9891−9898.
(26) Zhang, X. T.; Sui, Z. Y.; Xu, B.; Yue, S. F.; Luo, Y. J.; Zhan, W. C.; Liu, B. Mechanically Strong and Highly Conductive Graphene Aerogel and its Use as Electrodes for Electrochemical Power Sources. *J. Mater. Chem.* **2011**, *21*, 6494−6497.
(27) Xu, Y. X.; Sheng, K. X.; Li, C.; Shi, G. Q. Self-Assembled Graphene Hydrogel *via* a One-Step Hydrothermal Process. *ACS Nano* **2010**, *4*, 4324−4330.
(28) Guo, P.; Song, H.; Chen, X. Hollow Graphene Oxide Spheres Self-Assembled by W/O Emulsion. *J. Mater. Chem.* **2010**, *20*, 4867−4874.
(29) Lee, S. H.; Kim, H. W.; Hwang, J.; Lee, W.; Kwon, J.; Bielawski, C.; Ruoff, R.; Kim, S. Three-Dimensional Self-Assembly of Graphene Oxide Platelets into Mechanically Flexible Macroporous Carbon Films. *Angew. Chem., Int. Ed.* **2010**, *49*, 10084−10088.
(30) Hu, H.; Zhao, Z. B.; Wan, W. B.; Gogotsi, Y.; Qiu, J. S. Ultralight and Highly Compressible Graphene Aerogels. *Adv. Mater.* **2013**, *25*, 2219−2223.
(31) Cong, H. P.; Ren, X. C.; Wang, P.; Yu, S. H. Macroscopic Multifunctional Graphene-Based Hydrogels and Aerogels by a Metal Ion Induced Self-Assembly Process. *ACS Nano* **2012**, *6*, 2693−2703.
(32) Sui, Z.-Y.; Cui, Y.; Zhu, J.-H.; Han, B.-H. Preparation of Three-Dimensional Graphene Oxide−Polyethylenimine Porous Materials as Dye and Gas Adsorbents. *ACS Appl. Mater. Interfaces* **2013**, *5*, 9172−9179.
(33) Zhang, L. L.; Zhao, X.; Ji, H. X.; Stoller, M. D.; Lai, L. F.; Murali, S.; McDonnell, S.; Cleveger, B.; Wallace, R. M.; Ruoff, R. S. Nitrogen Doping of Graphene and Its Effect on Quantum Capacitance, and A New Insight on the Enhanced Capacitance of N-Doped Carbon. *Energy Environ. Sci.* **2012**, *5*, 9618−9625.
(34) Wang, H.; Zhang, C.; Liu, Z.; Wang, L.; Han, P.; Xu, H.; Zhang, K.; Dong, S.; Yao, J.; Cui, G. Nitrogen-Doped Graphene Nanosheets with Excellent Lithium Storage Properties. *J. Mater. Chem.* **2011**, *21*, 5430−5434.
(35) Ma, C.; Shao, X.; Cao, D. Nitrogen-Doped Graphene Nanosheets as Anode Materials for Lithium Ion Batteries: A First-Principles Study. *J. Mater. Chem.* **2012**, *22*, 8911−8915.
(36) Sheng, Z.-H.; Shao, L.; Chen, J.-J.; Bao, W.-J.; Wang, F.-B.; Xia, X.-H. Catalyst-Free Synthesis of Nitrogen-Doped Graphene *via* Thermal Annealing Graphite Oxide with Melamine and Its Excellent Electrocatalysis. *ACS Nano* **2011**, *5*, 4350−4358.
(37) Zhao, Y.; Hu, C. G.; Hu, Y.; Cheng, H. H.; Shi, G. Q.; Qu, L. T. A Versatile, Ultralight, Nitrogen-Doped Graphene Framework. *Angew. Chem., Int. Ed.* **2012**, *51*, 11371−11375.
(38) Yin, H.; Zhang, C.; Liu, F.; Hou, Y. Hybrid of Iron Nitride and Nitrogen-Doped Graphene Aerogel as Synergistic Catalyst for Oxygen Reduction Reaction. *Adv. Funct. Mater.* **2014**, *24*, 2930−2937.
(39) Zhang, J.; Li, R.; Li, Z.; Liu, J.; Gu, Z.; Wang, G. Synthesis of Nitrogen-Doped Activated Graphene Aerogel/Gold Nanoparticles and Its Application for Electrochemical Detection of Hydroquinone and *o*-Dihydroxybenzene. *Nanoscale* **2014**, *6*, 5458−5466.
(40) Hummers, W. S.; Offeman, R. E. Preparation of Graphitic Oxide. *J. Am. Chem. Soc.* **1958**, *80*, 1339−1339.
(41) Zu, S.-Z.; Han, B.-H. Aqueous Dispersion of Graphene Sheets Stabilized by Pluronic Copolymers: Formation of Supramolecular Hydrogel. *J. Phys. Chem. C* **2009**, *113*, 13651−13657.
(42) Chen, S.; Duan, J.; Tang, Y.; Qiao, S. Hybrid Hydrogels of Porous Graphene and Nickel Hydroxide as Advanced Supercapacitor Materials. *Chem.—Eur. J.* **2013**, *19*, 7118−7124.
(43) Zhou, D.; Cheng, Q.-Y.; Han, B.-H. Solvothermal Synthesis of Homogeneous Graphene Dispersion with High Concentration. *Carbon* **2011**, *49*, 3920−3927.
(44) Sun, L.; Tian, C.; Fu, Y.; Yang, Y.; Yin, J.; Wang, L.; Fu, H. Nitrogen-Doped Porous Graphitic Carbon as an Excellent Electrode Material for Advanced Supercapacitors. *Chem.—Eur. J.* **2014**, *20*, 564−574.
(45) Lai, L.; Chen, L.; Zhan, D.; Sun, L.; Liu, J.; Lim, S. H.; Poh, C. K.; Shen, Z.; Lin, J. One-Step Synthesis of NH_2-Graphene from in Situ Graphene-Oxide Reduction and Its Improved Electrochemical Properties. *Carbon* **2011**, *49*, 3250−3257.
(46) Ostrowski, J.; Eaves, J. The Tunable Hydrophobic Effect on Electrically Doped Graphene. *J. Phys. Chem. B* **2014**, *118*, 530−536.
(47) Lee, J. H.; Park, N.; Kim, B. G.; Jung, D. S.; Im, K.; Hur, J.; Choi, J. W. Restacking-Inhibited 3D Reduced Graphene Oxide for High Performance Supercapacitor Electrodes. *ACS Nano* **2013**, *7*, 9366−9374.

DOI: 10.1021/am5042065
ACS Appl. Mater. Interfaces 2015, 7, 1431−1438

(48) Simon, P.; Gogotsi, Y. Materials for Electrochemical Capacitors. *Nat. Mater.* **2008**, *7*, 845−854.
(49) Chen, S.; Zhu, J.; Wu, X.; Han, Q.; Wang, X. Graphene Oxide−MnO_2 Nanocomposites for Supercapacitors. *ACS Nano* **2010**, *4*, 2822−2830.
(50) Yu, G.; Hu, L.; Vosgueritchian, M.; Wang, H.; Xie, X.; McDonough, J. R.; Cui, X.; Cui, Y.; Bao, Z. Solution-Processed Graphene/MnO_2 Nanostructured Textiles for High-Performance Electrochemical Capacitors. *Nano Lett.* **2011**, *11*, 2905−2911.
(51) Wu, Q.; Xu, Y.; Yao, Z.; Liu, A.; Shi, G. Supercapacitors Based on Flexible Graphene/Polyaniline Nanofiber Composite Films. *ACS Nano* **2010**, *4*, 1963−1970.
(52) Chen, Q.; Luo, M.; Hammershøj, P.; Zhou, D.; Han, Y.; Laursen, B. W.; Yan, C.-G.; Han, B.-H. Microporous Polycarbazole with High Specific Surface Area for Gas Storage and Separation. *J. Am. Chem. Soc.* **2012**, *134*, 6084−6087.
(53) Srinivas, G.; Burress, J.; Yildirim, T. Graphene Oxide Derived Carbons (GODCs): Synthesis and Gas Adsorption Properties. *Energy Environ. Sci.* **2012**, *5*, 6453−6459.
(54) Burress, J. W.; Gadipelli, S.; Ford, J.; Simmons, J. M.; Zhou, W.; Yildirim, T. Graphene Oxide Framework Materials: Theoretical Predictions and Experimental Results. *Angew. Chem., Int. Ed.* **2010**, *49*, 8902−8904.
(55) Liu, D.-P.; Chen, Q.; Zhao, Y.-C.; Zhang, L.-M.; Qi, A.-D.; Han, B.-H. Fluorinated Porous Organic Polymers via Direct C−H Arylation Polycondensation. *ACS Macro Lett.* **2013**, *2*, 522−526.
(56) Lu, W.; Yuan, D.; Zhao, D.; Schilling, C. I.; Plietzsch, O.; Muller, T.; Bräse, S.; Guenther, J.; Blümel, J.; Krishna, R.; Li, Z.; Zhou, H.-C. Porous Polymer Networks: Synthesis, Porosity, and Applications in Gas Storage/Separation. *Chem. Mater.* **2010**, *22*, 5964−5972.

DOI: 10.1021/am5042065
ACS Appl. Mater. Interfaces 2015, 7, 1431−1438